Optics Letters

Demonstration of flat-band image transmission in optically induced Lieb photonic lattices

Shiqiang Xia,[1] Yi Hu,[1] Daohong Song,[1] Yuanyuan Zong,[1] Liqin Tang,[1,*] and Zhigang Chen[1,2,3]

[1]MOE Key Laboratory of Weak-Light Nonlinear Photonics, TEDA Applied Physics Institute and School of Physics, Nankai University, Tianjin 300457, China
[2]Department of Physics and Astronomy, San Francisco State University, San Francisco, California 94132, USA
[3]e-mail: zhigang@sfsu.edu
*Corresponding author: tanya@nankai.edu.cn

Received 14 December 2015; revised 9 February 2016; accepted 15 February 2016; posted 17 February 2016 (Doc. ID 255638); published 21 March 2016

We present a simple, yet effective, approach for optical induction of Lieb photonic lattices, which typically rely on the femtosecond laser writing technique. Such lattices are established by judiciously overlapping two sublattices (an "egg-crate" lattice and a square lattice) with different periodicities through a self-defocusing photorefractive medium. Furthermore, taking advantage of the superposition of localized flat-band states inherent in the Lieb lattices, we demonstrate distortion-free image transmission in such two-dimensional perovskite-like photonic structures. Our experimental observations find good agreement with numerical simulations.

OCIS codes: (130.2790) Guided waves; (230.0230) Optical devices; (070.7345) Wave propagation.

http://dx.doi.org/10.1364/OL.41.001435

In general, the Bloch modes of any periodic structure are extended indefinitely. However, a dispersionless energy band system allows for the existence of completely flat bands, and the corresponding linear Bloch modes are entirely localized degenerate states due to the destructive combination of extended wave functions [1]. This is particularly interesting because, in this case, waves can stay localized in the continuum, even without the presence of any defect [2], disorder [3] or nonlinearity [4]. Flat-band systems were originally explored and demonstrated in the study of ferromagnetism, which appears in a class of highly frustrated lattice models [5,6]. In recent years, flat-band physical phenomena have attracted ever-increasing attention, particularly in strongly correlated electron systems [7] due to their possible role in understanding and realization of topological insulators [8], fractional quantum Hall effect [9,10], and superconducting transitions [11]. Intriguing features also have been found when disorder and nonlinearity were introduced to interplay between degenerated states of the flat band [12–14]. The Lieb lattice, a face-centered square depleted lattice, is one of the simplest and best known platforms to demonstrate the features of flat-band systems. For example, very recently, Lieb photonic lattices (an array of evanescently coupled waveguides arranged in Lieb geometry) were realized with femtosecond laser writing techniques, where direct observations of diffractionless flat-band states became possible [15,16]. More interestingly, it was theoretically predicted that photonic flat-band modes might be used for diffraction-free image transmission [17]. Indeed, photonic lattices are ideal systems for active control of light propagation [2–4,18], and image transmission could be a typical example of application. Nevertheless, thus far, flat-band-based image transmission has not been demonstrated in experiment to the best of our knowledge. In addition, while various proposals have been put up for generation of optical Lieb lattices for cold atoms [19,20], Lieb lattices in photonics still rely on advanced femtosecond laser writing techniques [15,16,21,22].

In this Letter, we present a simple, yet effective, method for optical induction of Lieb photonic lattices, and we demonstrate the first experimental observation of distortion-free flat-band image transmission in such photonic structures. We show that a Lieb lattice intensity pattern can be constructed merely by overlapping two sublattices (an "egg-crate" lattice and a square lattice) with different periodicities, and the corresponding waveguide arrays with Lieb geometry can be optically induced in a photorefractive crystal with a self-defocusing nonlinearity. Our Lieb photonic lattices offer a convenient platform for probing the flat-band states. Furthermore, by linearly combining several localized flat-band eigenstates as a probe image, we experimentally observe the distortion-free flat-band image transmission in the optically induced Lieb photonic lattices.

The structure of Lieb photonic lattices is illustrated in Fig. 1(a) where each unit cell of the lattices consists of three sites, A, B, and C, as denoted by blue, green, and red points, respectively. The transmission band $\beta(k_x, k_y)$ for Bloch modes can be calculated from a paraxial Schrödinger-type equation describing light propagation in photonic lattices [2–4,15–18]:

$$i\frac{\partial\Psi(x,y,z)}{\partial z} = -\frac{1}{2k_0}\nabla^2\Psi(x,y,z) - \frac{k_0\Delta n(x,y)}{n_0}\Psi(x,y,z) \equiv H_0\Psi(x,y,z), \quad (1)$$

where Ψ is the electric field envelope of the probe beam, (x, y) are the transverse coordinates, z is the longitudinal propagation

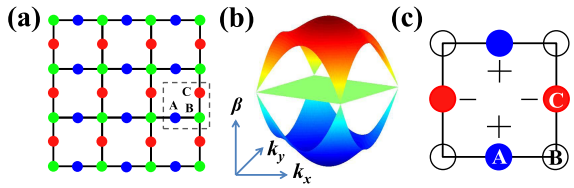

Fig. 1. (a) Lieb lattice with each unit cell (dashed square) consists of three lattice sites marked as A, B, and C. (b) Band structure in the tight-binding approximation. (c) Fundamental mode of flat-band localized degenerate eigenstates. Sites with nonzero amplitudes are denoted by solid (colored) circles; their amplitudes are the same, but the phases alternate between $\pm\pi$.

distance, ∇^2 is the transverse Laplacian operator, k_0 is the wavenumber within the medium, n_0 is the refractive index of the nonlinear medium, and Δn is the induced index change that forms the Lieb lattices. In Eq. (1), H_0 is the continuous Hamiltonian of the system, whose eigenvalues are the longitudinal wavenumbers (or the propagation constants). When only considering the hopping between the nearest-neighbor lattice sites, H_0 can be reasonably approximated by a tight-binding Hamiltonian. In this case, the Bloch modes of Lieb lattices are only distributed in three bands: a completely degenerated flat band centered between two curved ones, with all three bands intersecting at the high symmetric M points ($k_x = k_y = \pi$) of the first Brillouin zone (BZ) [Fig. 1(b)] [15,16,19,20]. Similar to honeycomb lattices [23,24], the curved bands are featured by the linear dispersion relation in the vicinity of M points (also called Dirac points), leading to intriguing phenomena such as conical diffraction [21], topological edge states [22], and pseudo-spin [25]. Another significant feature in this band structure is the presence of the flat band which comes from local interference effect. The flat band is topologically protected, and its eigenstates are strictly localized modes whose energy does not hop to the neighboring sites [1,15–17]. In any square plaquette of the lattice structure [Fig. 1(c)], a stationary localized mode can be formed by taking the four B sites with strictly zero amplitude, the other four sites with the same amplitude, but their phases alternate between $\pm\pi$. Light coupling from A and C sites onto B sites cancels out as a result of destructive interference, which is the reason why the flat-band mode will not be extended during linear propagation.

First, we discuss the idea of creating photonic Lieb lattices by use of optical induction, a well-established technique that translates a light intensity pattern into a positive (negative) refractive index change under a self-focusing (self-defocusing) nonlinearity in a photorefractive crystal [2–4,26]. To produce an optical lattice that is invariant along the propagation z-direction, a corresponding quasi-nondiffracting light pattern is constructed by interference of several plane waves. Unfortunately, one cannot find an appropriate interference pattern associated with a Lieb lattice due to its unique lattice site distribution [Fig. 1(a)]. Consequently, it is necessary to use the superposition of two or more optical patterns that are mutually incoherent to each other, as realized for one-dimensional superlattices [27]. In our Letter, we use two sets of lattice beams, namely an "egg-crate" lattice [28] and a square lattice, and their overlapping pattern does not change in the longitudinal direction. The constructing idea for Lieb lattices is illustrated numerically in Fig. 2. Both light-field patterns depicted in

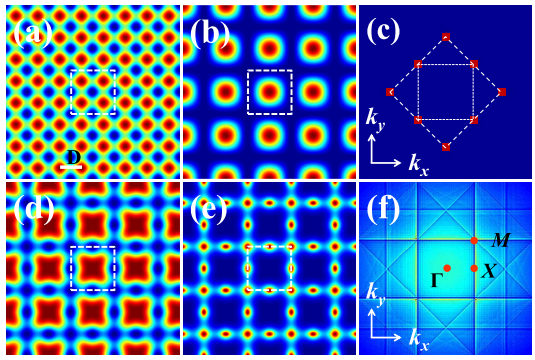

Fig. 2. Numerical results of optical induction of Lieb photonic lattices. (a) "Egg-crate" lattice pattern with a period of D. (b) Square lattice pattern with a period of 2D. (c) Fourier spectrum of the two lattice-forming beams, where the inner and outer squares represent the corresponding spectrum for lattices in (b) and (a), respectively. (d) Superimposed lattice pattern. (e) Optically induced waveguide arrays. (f) Corresponding extended BZ with the high symmetry points marked by red points. Dashed squares in left four panels mark the same overlapping square zone.

Figs. 2(a) and 2(b) are produced by four-beam interference, whose superimposed spatial spectrum and intensity are shown in Figs. 2(c) and 2(d), respectively. More specifically, by applying a proper $\pi/2$ phase difference among the four lattice-inducing beams, a perfect "egg-crate" light pattern can be constructed [Fig. 2(a)]. Mathematically, its complex amplitude is expressed as $V_e(x,y) = V_1[\exp(ikx) + \exp(iky + i\pi/2) + \exp(-ikx + i\pi) + \exp(-iky + 3i\pi/2)]$, having minima at lattice sites $R = (mD; nD)$ (m and n are integers) [28]. Here, $k = \pi/D$ is the optical wave vector, where D is the "egg-crate" lattice constant. As for the square lattices, there is no additional phase difference between the four beams, i.e., $V_s(x,y) = V_2 \sum_{\sigma=\pm1} \exp(i\sigma k(x \pm y)/2)$. ($V_1$ and V_2 correspond to the amplitudes of the two lattice-inducing beams.) Note that these beams are properly titled to make sure that the intensity maxima of the square pattern match the intensity minima of the "egg-crate" pattern. The resulting optical field, formed by incoherent overlapping the two lattice waves, could be represented by $I(x,y) = |V_e|^2 + |V_s|^2$. The intensity pattern $I(x,y)$ for $V_1 = V_2 = 1$ [Fig. 2(d)] reveals that the intensity minima form the structure of the Lieb lattices. Therefore, an optical Lieb lattice can be induced by employing the self-defocusing nonlinearity [Fig. 2(e)]. To further characterize the structure of the lattices, we numerically calculate its BZ which has a structure in Fourier space similar to that of a square lattice due to their similarity in symmetry [Fig. 2(f)].

For the experimental demonstration, we use a continuous wave (CW) laser operating at 488 nm for both inducing and probing the Lieb lattices and a strontium barium niobate (SBN) crystal as the photorefractive material which provides a self-defocusing nonlinearity under a proper bias field. The experimental setup is similar to that used in [24] and the same as the method for generation of one-dimensional superlattices [27]; now two ordinarily polarized partially coherent beams, each passing through an amplitude mask, are used for generating the "egg-crate" and square lattice beams. To minimize the effect of photorefractive anisotropy in the crystal, the two sets of lattice beams are rotated at 45° relative to the horizontal-vertical axes.

Figure 3 shows typical experimental results corresponding to Fig. 2. The period of the "egg-crate" lattice field [Fig. 3(a)] is 26 μm, and that of the square lattice [Fig. 3(b)] is 52 μm. The ratio between the peak intensities of the two lattices is about 1:1.5. The spatial spectrum and intensity of their incoherent superposition are shown in Figs. 3(c) and 3(d), respectively. Both ensure and reveal that the intensity maxima of the square pattern exactly fill in the intensity minima of the "egg-crate" pattern. To visualize the induced Lieb lattice experimentally, we illuminate a weak extraordinarily polarized quasi-plane wave to probe the waveguide array induced in the crystal. At the back facet of the crystal, we can see that the otherwise uniform probe beam is guided into each lattice site, indicating a perfect Lieb lattice waveguide structure already established [Fig. 3(e)]. As seen in Figs. 2(e) and 3(e), our induced Lieb lattices are more uniform in both directions along the lattice principal axes, as compared to those fabricated using the femtosecond laser writing technique which are somewhat anisotropic [15,16]. The BZ spectrum of the induced lattices is measured by using the BZ spectroscopy [Fig. 3(f)] [29]. Six dark stripes (shown by two horizontal and four oblique dashed lines) appear in the power spectrum of the probe beam due to Bragg reflections near the boundaries of the BZs of the lattices. Compared with the calculated results [Fig. 2(f)], only the first two BZs are revealed. The first BZ is apparent, while the second comes into view partially since two vertical lines are missing as a result of the anisotropy of the crystal [28].

Next, we discuss excitation of flat-band modes and observation of distortion-free image transmission in the optically induced Lieb photonic lattices. As mentioned above, a flat band is composed of entirely degenerate localized states. As a result of this degeneracy, the superposition of these states is also an eigenstate of the system and, therefore, displays no diffraction. Thus, any desired image constructed as a combination of several degenerate modes will propagate stably. To demonstrate this feature, let us first look at the propagation dynamics of the fundamental flat-band mode [Fig. 1(c)] using the paraxial equation [Eq. (1)]. Simulation results are shown in the top row of Fig. 4. The lattice constant is set to 26 μm to match the experiment parameter. A quadruple beam with out-of-phase structure characterizing the fundamental flat-band mode is employed as the input that excites only lattice sites A and C as shown in Fig. 4(a). Figures 4(c) and 4(d) show the corresponding linear

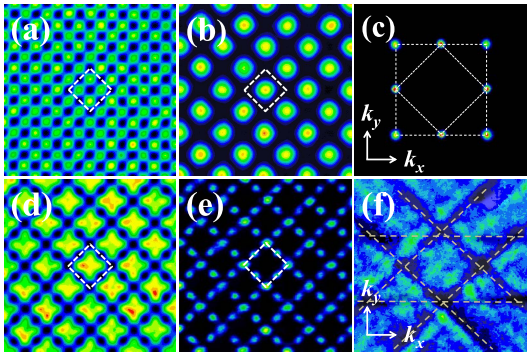

Fig. 3. Experimental results of optical induction of Lieb photonic lattices in a 10 mm long nonlinear crystal corresponding to Fig. 2. The principal axes of the lattices are oriented in diagonal (rather than horizontal-vertical) directions for reasons discussed in the text.

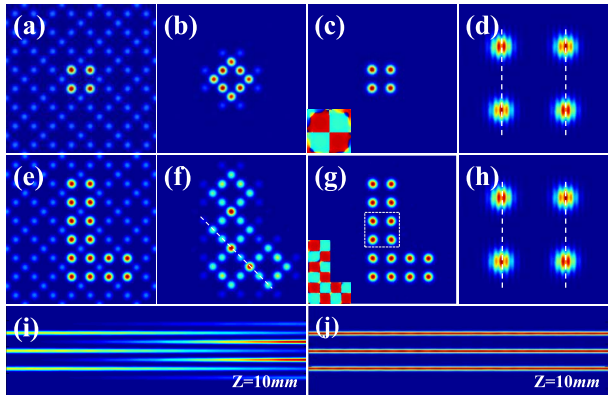

Fig. 4. Numerical results of linear propagation of a fundamental flat-band mode (top row) and an L-shaped image (middle row) through Lieb photonic lattices. (a), (e) Input. (b), (f) In-phase output of discrete diffraction. (c), (g) Out-of-phase output of the preserving pattern. (d), (h) Interferogram of (c) and (g) (zoomed-in for better visualization, and only the interference pattern of the central four sites in (g) is shown). (i), (j) Side view of beam propagation corresponding to (f) and (g) along the direction of the dashed white line in (f).

output and interference pattern after propagating 10 mm through the crystal (which corresponds to about a 1.5 coupling length in the lattices). It can be clearly seen that the linear output stays well localized in the initially excited four lattice sites [Fig. 4(c)], experiencing no diffraction during propagation. Moreover, both phase diagram [inset in Fig. 4(c)] and phase measurement [Fig. 4(d)] by interfering the output with an inclined plane wave indicate that the initial out-of-phase structure is also well preserved. For comparison, if the input quadruple beam is initially in-phase instead, the flat-band mode cannot be excited, and the output displays discrete diffraction with beam intensity evolving into several nearby lattice sites [Fig. 4(b)]. Interestingly, as a specific example to demonstrate the distortion-free flat-band image transmission, we keep other parameters unchanged, but construct a letter "L" as a probe beam to excite the lattices. Results are shown in the middle row of Fig. 4. For simplicity, the letter "L" is overlaid only by a train of four fundamental modes with no overlapping region [Fig. 4(e)]. When the image is composed of the fundamental flat-band modes in which all sites are kept out of phase, a distortion-free image transmission is realized [Fig. 4(g)], and the phase structure is also well preserved [Figs. 4(g) and 4(h)]. However, this is certainly not the case when all the sites of the image are in phase [Fig. 4(f)]. Instead, in the latter case, the input image no longer can be preserved. Figures 4(i) and 4(j) in the bottom row of Fig. 4 show the side view of propagation corresponding to Figs. 4(f) and 4(g), respectively, which reveals clearly the distorted and undistorted image transmission. It should be noted that for lattice constant and propagation length considered in our Letter, the effect of next-nearest neighbor interactions appears to be negligible due to the weak coupling interaction coming from well-separated lattices. We perform simulations for different lattice constants and find that the fundamental localized mode cannot be exited after 10 mm propagation in lattices with $D \leq 22$ μm. This is because in the strong coupling region, the next-nearest neighbor coupling is non-negligible, and the flat band cannot preserve [16].

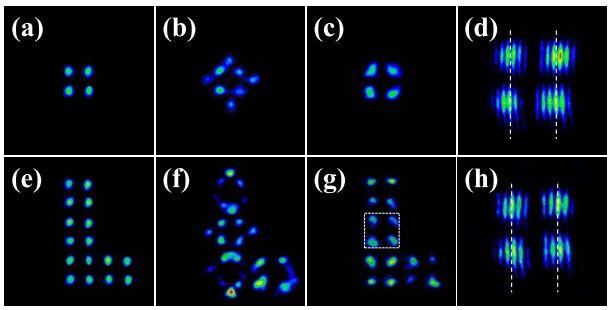

Fig. 5. Experimental results of linear propagation of a flat-band mode (top row) and an image (bottom row) through Lieb photonic lattices. (a), (e) Input. (b), (f) In-phase output. (c), (g) Out-of-phase output. (d), (h) Zoom-in interferogram corresponding to (c) and (g), respectively.

Finally, we present experimental results of the flat-band-based text or image transmission. To generate the input probe beams as shown in Figs. 4(a) and 4(e), a phase-only spatial light modulator (SLM) is used so that we can control the intensity pattern, as well as the phase structure of the probe beam. We simultaneously encode the amplitude and phase information onto the SLM by designing a hologram (phase mask) consisting of several phase gratings arranged in a square or L-shaped structure. Then, an extraordinarily polarized quasi-plane wave is sent to the SLM, and the first order of the diffracted light whose intensity distribution has a desired pattern is imaged to the facet of the crystal as a probe beam. The size of each light spot of the probe beam at the lattice input facet is controlled by the imaging lens, and the spacing between the light spots is controlled via adjusting the phase gratings. At the same time, the relative phase between the spots is controlled by changing the relative locations of the gratings. Once the probe beam is shaped for the desired exciting condition, it is sent into the induced Lieb lattices, and the output pattern is monitored in the back facet of the crystal. Typical experimental results are shown in Fig. 5. In Figs. 5(b) and 5(f), we observe that the beam profiles with uniform phase structure are destroyed and diffract to the nearby lattice sites. However, the intensity patterns [Figs. 5(c) and 5(g)] and the interferograms [Figs. 5(d) and 5(h)] clearly reveal that the out-of phase inputs can be well preserved after 10 mm of propagation, indicating that this type of localization relies on the phase structure of the input. The contrast of the discrete diffraction and diffractionless patterns also reveal that the localization indeed results from flat-band modes rather than simple waveguiding. Overall, our experimental results agree well with our simulations.

Before closing, we would like to mention that the letter "L" also can be constructed with zero amplitude sites in the superposition region of the flat-band modes as was demonstrated in Kagome lattices [17]. With the combination of these two superposition methods, one can construct any desired text, symbol, or image as the superposition of the flat-band modes that can propagate robustly in the flat-band photonic lattices.

In summary, we have successfully developed a simple yet effective approach to optically induce Lieb photonic lattices and experimentally observed the distortion-free flat-band image transmission in the resulting lattices. The diffractionless flat-band states are unique to flat-band systems and provide a new type of wave localization. The concept might be adopted for further studies in other systems beyond optics.

Funding. 973 Programs (2013CB328702, 2013CB632703); National Natural Science Foundation of China (NSFC) (11304165, 11504186, 61575098); 111 Project in China (B07013).

REFERENCES

1. D. L. Bergman, C. Wu, and L. Balents, Phys. Rev. B **78**, 125104 (2008).
2. I. Makasyuk, Z. Chen, and J. Yang, Phys. Rev. Lett. **96**, 223903 (2006).
3. T. Schwartz, G. Bartal, S. Fishman, and M. Segev, Nature **446**, 52 (2007).
4. J. W. Fleischer, M. Segev, N. K. Efremidis, and D. N. Christodoulides, Nature **422**, 147 (2003).
5. E. H. Lieb, Phys. Rev. Lett. **62**, 1201 (1989).
6. A. Mielke, J. Phys. A **24**, 3311 (1991).
7. O. Derzhko, J. Richter, and M. Maksymenko, Int. J. Mod. Phys. B **29**, 1530007 (2015).
8. C. Weeks and M. Franz, Phys. Rev. B **82**, 085310 (2010).
9. E. Tang, J.-W. Mei, and X.-G. Wen, Phys. Rev. Lett. **106**, 236802 (2011).
10. T. Neupert, L. Santos, C. Chamon, and C. Mudry, Phys. Rev. Lett. **106**, 236804 (2011).
11. V. I. Iglovikov, F. Hébert, B. Grémaud, G. G. Batrouni, and R. T. Scalettar, Phys. Rev. B **90**, 094506 (2014).
12. D. Leykam, S. Flach, O. Bahat-Treidel, and A. S. Desyatnikov, Phys. Rev. B **88**, 224203 (2013).
13. S. Flach, D. Leykam, J. D. Bodyfelt, P. Matthies, and A. S. Desyatnikov, Eur. Phys. Lett. **105**, 30001 (2014).
14. D. Leykam, J. D. Bodyfelt, A. S. Desyatnikov, and S. Flach, "Localization of weakly disordered flat band states," arXiv:1601.03784 (2016).
15. R. A. Vicencio, C. Cantillano, L. Morales-Inostroza, B. Real, C. Mejía-Cortés, S. Weimann, A. Szameit, and M. I. Molina, Phys. Rev. Lett. **114**, 245503 (2015).
16. S. Mukherjee, A. Spracklen, D. Choudhury, N. Goldman, P. Öhberg, E. Andersson, and R. R. Thomson, Phys. Rev. Lett. **114**, 245504 (2015).
17. R. A. Vicencio and C. Mejía-Cortés, J. Opt. **16**, 015706 (2014).
18. F. Lederer, G. I. Stegeman, D. N. Christodoulides, G. Assanto, M. Segev, and Y. Silberberg, Phys. Rep. **463**, 1 (2008).
19. R. Shen, L. B. Shao, B. Wang, and D. Y. Xing, Phys. Rev. B **81**, 041410 (2010).
20. S. Taie, H. Ozawa, T. Ichinose, T. Nishio, S. Nakajima, and Y. Takahashi, Sci. Adv. **1**, e1500854 (2015).
21. F. Diebel, D. Leykam, S. Kroesen, C. Denz, and A. S. Desyatnikov, in *Advanced Photonics*, OSA Technical Digest (online) (Optical Society of America, 2014), paper NW3A.1.
22. D. Guzmán-Silva, C. Mejía-Cortés, M. A. Bandres, M. C. Rechtsman, S. Weimann, S. Nolte, M. Segev, A. Szameit, and R. A. Vicencio, New J. Phys. **16**, 063061 (2014).
23. O. Peleg, G. Bartal, B. Freedman, O. Manela, M. Segev, and D. N. Christodoulides, Phys. Rev. Lett. **98**, 103901 (2007).
24. D. Song, V. Paltoglou, S. Liu, Y. Zhu, D. Gallardo, L. Tang, J. Xu, M. Ablowitz, N. K. Efremidis, and Z. Chen, Nat. Commun. **6**, 6272 (2015).
25. D. Leykam, O. Bahat-Treidel, and A. S. Desyatnikov, Phys. Rev. A **86**, 031805 (2012).
26. N. K. Efremidis, S. Sears, D. N. Christodoulides, J. W. Fleischer, and M. Segev, Phys. Rev. E **66**, 046602 (2002).
27. N. Malkova, I. Hromada, X. Wang, G. Bryant, and Z. Chen, Opt. Lett. **34**, 1633 (2009).
28. P. Zhang, S. Liu, C. Lou, F. Xiao, X. Wang, J. Zhao, J. Xu, and Z. Chen, Phys. Rev. A **81**, 041801 (2010).
29. G. Bartal, O. Cohen, H. Buljan, J. W. Fleischer, O. Manela, and M. Segev, Phys. Rev. Lett. **94**, 163902 (2005).